An RNA Molecule Derived From Sendai Virus DI Particles Induces Antitumor Immunity and Cancer Cell-selective Apoptosis

Li-Wen Liu[1], Tomoyuki Nishikawa[1] and Yasufumi Kaneda[1]

[1]*Division of Gene Therapy Science, Graduate School of Medicine, Osaka University, Osaka, Japan*

Inactivated Sendai virus (hemagglutinating virus of Japan; HVJ) envelope (HVJ-E) induces anticancer immunity and cancer cell-selective apoptosis through the recognition of viral RNA genome fragments by retinoic acid-inducible gene-I (RIG-I). Here, we discovered that the "copy-back" type of defective-interfering (DI) particles that exist in the Cantell strain of HVJ induced the human PC3 prostate cancer cell death more effectively than the Sendai/52 strain or Cantell strain, which contain fewer DI particles. DI particle genomic RNA (~550 bases) activated proapoptotic genes such as *Noxa* and/or TNF-related apoptosis-inducing ligand (*TRAIL*) in human prostate cancer cells to induce cancer cell-selective apoptosis. DI particle-derived RNA was synthesized by *in vitro* transcription (*in vitro* transcribed (IVT)-B2). IVT-B2 RNA, which has a double-stranded region in its secondary structure, promoted a stronger anticancer effect than IVT-HN RNA, which does not have a double-stranded region in its secondary structure. The intratumoral transfection of IVT-B2 significantly reduced the volume of a human prostate tumor and induced tumor cell apoptosis in the xenograft mouse model. Moreover, the involvement of natural killer (NK) cells in IVT-B2-RNA-induced anticancer effects was also suggested. These findings provide a novel nucleic acid medicine for the treatment of cancer.

Received 21 May 2015; accepted 23 October 2015; advance online publication 8 December 2015. doi:10.1038/mt.2015.201

INTRODUCTION

Cancer therapy has been widely explored for many years. However, the commonly used cancer treatments such as chemotherapy and radiation therapy occasionally induce severe side effects and/or drug resistance. The systemic administration of anticancer drugs occasionally attacks not only neoplastic cells but also somatic cells. Therefore, the development of a novel treatment that is more efficient in suppressing cancer cells with minimal side effects is an extremely important issue.

Prostate cancer is the most prevalent cancer among males in the United States. The current treatments for prostate cancer induce various urinary and systemic side effects.[1] Moreover, in its initial stages, prostate cancer is responsive to androgen deprivation therapy, which is accomplished by surgical or medical castration. However, subsequent to androgen deprivation therapy, prostate cancers relapse and become castration resistant in many cases despite reduced circulating testosterone levels.[2]

Currently, various types of oncolytic virotherapy have been developed. Some viruses, such as Newcastle disease virus (NDV) and human reovirus, revealed that tumor cells were preferentially infected[3,4]; other genetically engineered viruses, for example, adenoviruses with E1B-55-kDa or E1A-CR2 deletions, have also been investigated for cancer treatment.[5–7] However, live and attenuated virus treatments in cancer still have safety problems. We have already reported that a nonreplicating Sendai virus (hemagglutinating virus of Japan) envelope (HVJ-E) stimulates anticancer immunity and cancer cell-selective apoptosis.[8–11] HVJ-E treatment induced anticancer immunity through the inactivation of Tregs (regulatory T cells) and the promotion of natural killer (NK) cell activation, which is mediated by cytokines and chemokines such as IL6 and CXCL10.[8,9] In cancer cells, the mechanism of the anticancer effect was that HVJ-E RNA genome fragments are recognized by the cytoplasmic RNA receptor retinoic acid-inducible gene-I (RIG-I) and trigger the downstream mitochondrial antiviral signaling (MAVS) protein to activate various transcription factors, such as interferon regulatory factor (IRF) 3 and 7. Through this signaling pathway, cancer cell-selective apoptosis was induced by activating proapoptotic genes such as TNF-related apoptosis-inducing ligand (*TRAIL*) and *Noxa*.[10–12] RIG-I is a cytoplasmic pattern recognition receptor that is responsible for the detection of pathogenic nucleic acids. Previous studies demonstrated that RIG-I is essential for interferon (IFN) production in innate antiviral responses to several RNA viruses, including the paramyxoviruses, influenza virus, and Japanese encephalitis virus.[13,14] HVJ Cantell strain-mediated dendritic cell (DC) maturation requires signaling through RIG-I.[15] In addition, a study has demonstrated that RIG-I mainly recognizes shorter double-stranded RNA (dsRNA; ~300 bp to 1 kb), while Melanoma Differentiation-Associated protein 5 (MDA5) is responsible for recognizing longer dsRNA (>1 kb) triggering downstream type-I IFNs during antiviral responses.[16] It has been proven that the carboxy-terminal domain of RIG-I binds to 5′-triphosphate dsRNA or ssRNA. Compared with the overhangs of dsRNA and ssRNA with 5′-triphosphate, the blunt dsRNA

Correspondence: Yasufumi Kaneda, Division of Gene Therapy Science, Graduate School of Medicine, Osaka University, 2-2 Yamada-oka, Suita, Osaka 565–0871, Japan. E-mail: kaneday@gts.med.osaka-u.ac.jp

with 5′-triphosphate displays the highest affinity for RIG-I and is a very effective activator of RIG-I.[17,18]

The virus RNA pathogen-associated molecular patterns characteristics of oncolytic virotherapy are not well understood. In a previous study, the Cantell strain of HVJ promoted greater DC maturation and type-I IFN production than the Sendai/52 strain (Z strain) of HVJ or a dose of influenza virus. It has been proven that viral defective-interfering (DI) particles in the Cantell strain of HVJ contribute to the Toll-like receptor (TLR)-independent immunostimulatory ability.[15] Cantell DI particles contain incomplete viral genomes and are generated through errors in viral replication.[19] During viral replication, Cantell strain HVJ DI genomes, which replace the weaker 3′ end genomic replication promoter in their minus strands with the stronger antigenomic promoter, are known as a "copy-back" type of DI genome.[20] The copy-back type of DI particle RNA genome in the Cantell strain of HVJ has complementary termini (~100 bases), which forms the stem region of the frying pan–shaped secondary RNA structure and exhibits the highest binding affinity to RIG-I.[21,22]

In this study, the virus RNA pathogen-associated molecular patterns characteristics of those in cancer treatment were clarified through investigating the DI particle RNA genome with respect to its anticancer effect. The DI RNA genome of the Cantell strain of HVJ played an important role in the induction of IFN-β, the expression of proapoptotic proteins, and the promotion of cancer cell death. We also demonstrated that IVT DI RNA with 5′-triphosphate according to the Cantell HVJ DI genome sequence would be an effective anticancer reagent by inducing both antitumor immunity and cancer-cell apoptosis.

RESULTS

β-Propiolactone-treated Cantell strain HVJ induced the RIG-I/MAVS signaling pathway and proapoptotic proteins expression in cancer cells

To determine the RNA genomic component of inactivated HVJ particles, isolated viral RNAs were examined via electrophoresis. The viral replication of HVJ was inactivated by β-propiolactone (βPL) treatment without breaking down the RNA genome. The complete viral genome RNA (~15 kb) was found in both the βPL-Neo-Z strain HVJ (βPL-Neo-Z-HVJ) and βPL-Cantell strain HVJ (βPL-Cantell-HVJ), but only the βPL-Cantell-HVJ presented the DI RNA genome, which

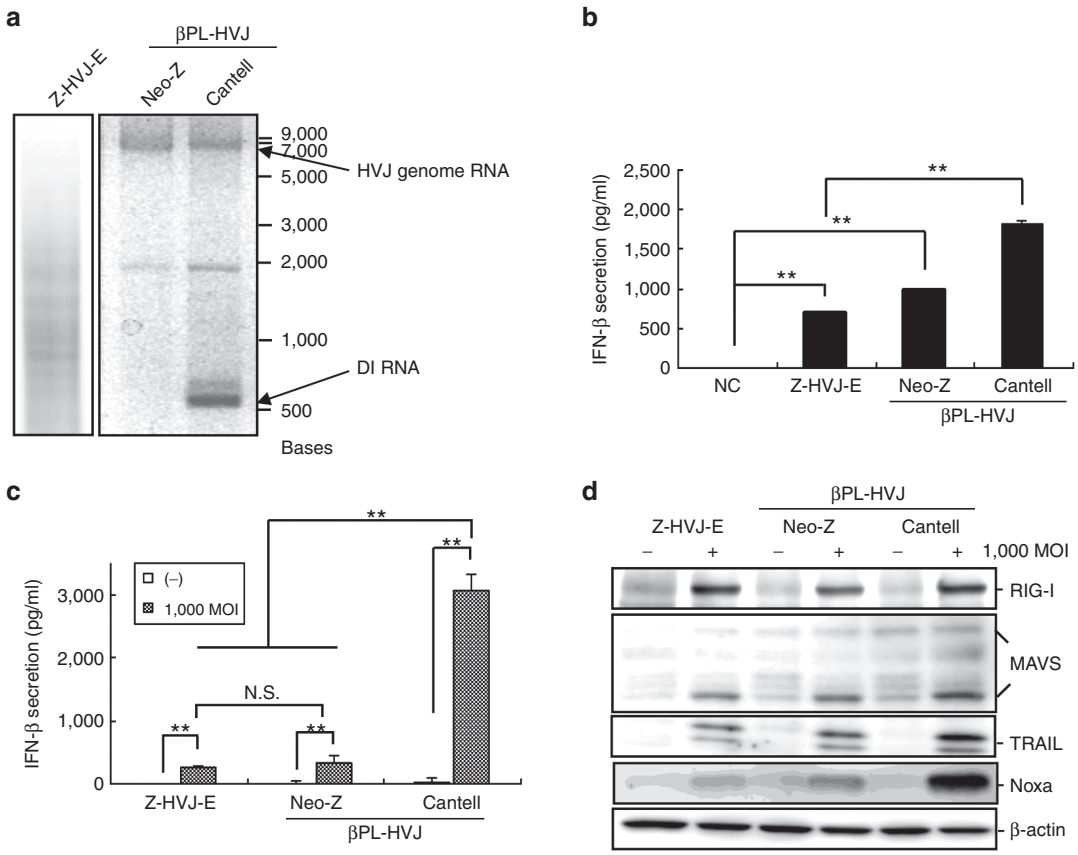

Figure 1 Inactivated-Cantell strain HVJ stimulated the RIG-I/MAVS signal pathway and proapoptotic proteins expression in cancer cells. (**a**) Inactivated-HVJ RNAs were isolated from UV-irradiated Z strain HVJ (Z-HVJ-E), β-propiolactone (βPL)-treated Neo-Z or Cantell strain HVJ. The upper arrow indicates the HVJ genome RNA (~15,000 nucleotides); the lower arrow indicates the DI genome RNA (~500 nucleotides). (**b**) Mouse splenocytes were stimulated with Z-HVJ-E, βPL-Neo-Z, or βPL-Cantell strain HVJ at a multiplicity of infection (MOI) of 1,000. Mouse IFN-β secretion was detected via an ELISA at 72 hours after inactivated HVJ treatment. "NC" indicates cells that were treated with phosphate-buffered saline only. (**c**) PC3 cells were treated with inactivated HVJ at 1,000 MOI. IFN-β secretion was detected via an ELISA 24 hours later. The mean values ± SD are shown ($n = 4$). *$P < 0.05$. **$P < 0.01$. (**d**) RIG-I, MAVS, Noxa, and TRAIL expression in PC3 cells was examined by western blot analysis. ELISA, enzyme-linked immunosorbent assay.

had a much lower molecular weight than the genomic RNA (**Figure 1a**, ~500 nucleotides). The Z strain HVJ-E (Z-HVJ-E) was treated with UV irradiation, and the genomic RNA fragments of various sizes are depicted in **Figure 1a**. The expression of IFN-β in mouse splenocytes was analyzed (**Figure 1b**). βPL-Cantell-HVJ treated splenocytes induced a significantly higher level of IFN-β production than that observed in UV-irradiated Z-HVJ-E- and βPL-Neo-Z-HVJ-treated splenocytes. In addition, the βPL-Cantell-HVJ treatment promoted a higher level of IFN-β secretion in PC3 prostate cancer cells (**Figure 1c**) and A549 lung cancer cells (**Supplementary Figure S1**) than treatment of the cells with Z-HVJ-E or βPL-Neo-Z-HVJ. The protein expression levels of RIG, MAVS, TRAIL, and Noxa in PC3 cells were evaluated. As shown in **Figure 1d**, RIG-I and MAVS were upregulated by treatment with Z-HVJ-E, βPL-Neo-Z-HVJ, or βPL-Cantell-HVJ. βPL-Cantell-HVJ induced significantly more Noxa and TRAIL expression than Z-HVJ-E or βPL-Neo-Z-HVJ in PC3 cells. Previous studies proved that RNA fragments of UV-irradiated Z strain HVJ-E promote cell apoptosis via the cytoplasmic RNA receptor, RIG-I.[12] Additionally, HVJ DI RNA was observed to preferentially associate with RIG-I in the context of infections.[23] Then, we examined whether the DI RNA genome in the Cantell strain of HVJ could be the primary inducer of proapoptotic protein expression in cancer cells.

The viral RNA from the DI particle-rich fraction was more efficient than Z-HVJ-E or Cantell strain βPL-HVJ RNA for cancer cell-selective induction of Noxa and TRAIL

The βPL-Cantell-HVJ (βPL-Can-total) was purified from Cantell strain HVJ-infected chorioallantoic fluid by centrifugation after the inactivation of viral replication. Because DI particles have a lower density than the standard HVJ particles, the supernatant fraction of the chorioallantoic fluid contained a higher DI particle/standard viral particle ratio (βPL-Can-DI-rich) after the centrifugation.[15,24] Viral RNA was isolated from the βPL-Can-total or βPL-Can-DI-rich viral fractions; a higher ratio of DI/complete genomic RNA was observed in the βPL-Can-DI-rich fraction (**Figure 2a**). A smaller amount of RNA was contained in the βPL-Can-DI-rich group than in the βPL-Can-total and Z-HVJ-E samples because more DI particles were present in the Can-DI-rich fraction than the standard HVJ fractions (**Supplementary Figure S2**). The βPL-Cantell strain HVJ RNAs or UV-irradiated Z HVJ-E RNA was transfected into PC3 cells (**Figure 2a**,**b**). The induction of PC3 cell death that was caused by the viral RNA transfection from the βPL-Can-DI-rich fraction was more effective than the Z-HVJ-E or βPL-Can-total RNA treatment groups. In addition, cancer cell–specific induction of proapoptotic protein was examined (**Figure 2c**). In the PC3 cells, transfection with HVJ RNA

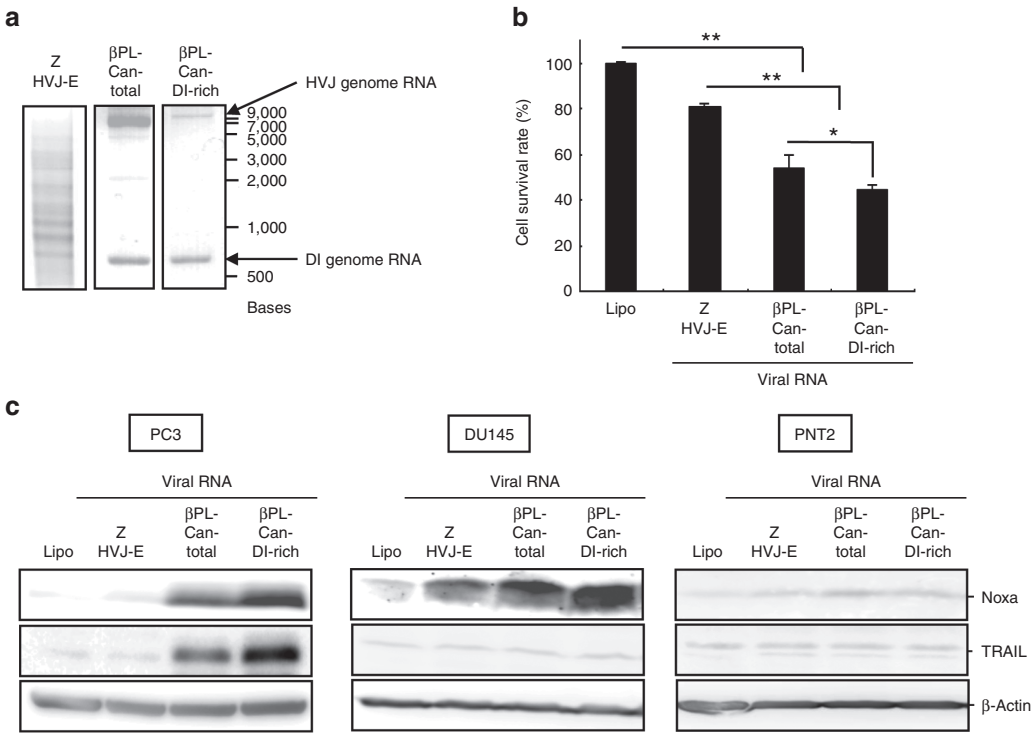

Figure 2 The HVJ RNA from the DI particle-rich fraction was more efficient than Z or Cantell stain HVJ RNA for promoting cancer cell death and cancer cell-selective induction of Noxa and TRAIL. (**a**) HVJ RNAs were isolated from Z-HVJ-E, β-propiolactone (βPL)-treated Cantell strain HVJ (βPL-Can-total), or the Cantell strain DI particle-rich fraction (βPL-Can-DI-rich). The upper arrow indicates the size of the HVJ genome RNA; the lower arrow indicates the size of the DI genome RNA. (**b**) The HVJ RNAs (0.067 ng/ml) were transfected into PC3 cells. Cell survival was assessed with a MTS assay at 48 hours after RNA transfection. (**c**) HVJ RNAs were transfected into PC3, DU145, or PNT2 cells. The expression levels of Noxa and TRAIL were then assessed by western blot analysis 24 hours after RNA transfection. "Lipo" indicates cells that were treated with Lipofectamine RNAiMAX without RNA. *$P < 0.05$; **$P < 0.01$. MTS, 3-(4,5-dimethyl-2-yl)-5-(3-carboxymethoxyphenyl)-2-(4-sulfophenyl)-2H-tetrazolium, inner salt.

from the βPL-Can-DI-rich fraction increased TRAIL expression; and Noxa was upregulated to a higher degree in both the PC3 and DU145 prostate cancer cells that were transfected with RNA from the βPL-Can-DI-rich fraction. However, neither of the proapoptotic proteins, Noxa and TRAIL, was induced in noncancerous prostate epithelial PNT2 cells after transfection with the same inactivated HVJ RNAs (**Figure 2c**). These results suggest that DI RNA genome from the Cantell strain of HVJ could play a role in promoting cancer cell death and inducing cancer cell-specific expression of proapototic proteins.

The effect of gel-extracted Cantell strain HVJ DI RNA on cancer cells

Next, the role of the DI RNA genome in the anticancer effect was confirmed with gel-extracted DI RNA. Cantell strain HVJ DI RNA (DI) and whole genomic RNA (G) were separated by agarose gel electrophoresis to purify each RNA (**Figure 3a**). DI RNA-transfected PC3 cells expressed a significantly higher level of IFN-β than the liposome control and whole-genome RNA-transfected cells (**Figure 3b**). Moreover, transfection with the gel-extracted DI RNA significantly induced cell death compared with the Cantell whole-genome RNA transfected PC3 cells (**Figure 3c**). The expression levels of RIG-I/MAVS-related proapoptotic proteins were evaluated in PC3 cells (**Figure 3d**). Higher levels of Noxa and TRAIL expression were induced by transfection with the gel-extracted DI RNA. Furthermore, caspase-3 expression, a critical apoptosis executioner, was also analyzed in PC3 cells. The expression of the active form of caspase-3 was significantly upregulated by transfection with the gel-extracted DI RNA (**Figure 3d**). Similar results were observed in MDA-MB-231 cells

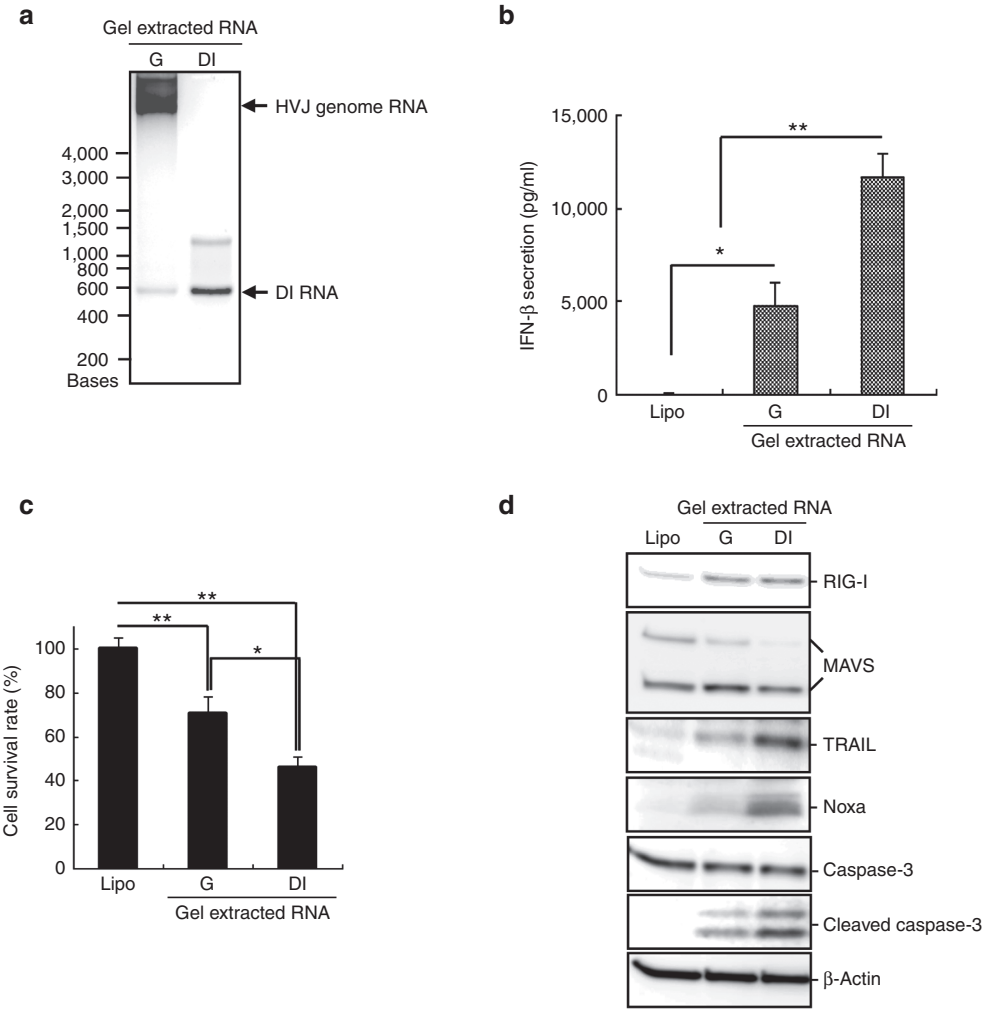

Figure 3 Gel-extracted DI RNA was more efficient than Cantell strain HVJ whole-genome RNA for cancer cell killing and the induction of apoptosis-related proteins expression. (**a**) HVJ RNA was isolated from β-propiolactone (βPL)-treated Cantell strain HVJ and was separated by RNase-free agarose gel electrophoresis. The Cantell HVJ whole genome RNA or DI genome RNA was extracted from the agarose gel and was confirmed by RNase-free agarose gel electrophoresis. Lane 1: gel-extracted Cantell HVJ whole genome RNA (G); lane 2: gel-extracted Cantell HVJ DI genome RNA (DI). The upper arrow indicates the size of the HVJ whole-genome RNA; the lower arrow indicates the size of the DI genome RNA. (**b**) The gel-extracted Cantell HVJ whole genome or the DI RNA (0.067 ng/ml) was transfected into PC3 cells. IFN-β secretion was detected in the cell culture medium with an ELISA 48 hours after RNA transfection. The mean ± SD is shown ($n = 3$). (**c**) The gel-extracted Cantell HVJ whole genome or the DI RNA (0.067 ng/ml) was transfected into PC3 cells. The cell survival was assessed with a MTS assay 48 hours after RNA transfection. The mean ± SD is shown ($n = 3$). *$P < 0.05$; **$P < 0.01$. (**d**) Expression levels of RIG-I, MAVS, Noxa, TRAIL, and caspase-3 in the PC3 cells were measured by western blot analysis 24 hours after RNA transfection. ELISA, enzyme-linked immunosorbent assay. MTS, 3-(4,5-dimethyl-2-yl)-5-(3-carboxymethoxyphenyl)-2-(4-sulfophenyl)-2H-tetrazolium, inner salt.

that were transfected with the gel-extracted Cantell strain HVJ DI and whole genomic RNA (**Supplementary Figure S3**). The same amount of gel-extracted DI RNA induced a higher level of expression of those apoptosis-related proteins and more cell death than the whole-genome RNA did. These results suggest that in the Cantell strain HVJ, the DI RNA genome rather than the standard whole genomic RNA plays a predominant role in the induction of IFN-β and RIG/MAVS signal-related proapoptotic proteins expression in cancer cells.

IVT-DI RNA-induced cancer cell death and the expression of apoptosis-related proteins in PC3 cells

Next, we examined whether the specific secondary structure of the DI RNA genome stimulates the RIG-I/MAVS downstream-related cancer suppressive pathways using HVJ-derived IVT RNAs. DI RNA (IVT-B2) and control RNA (IVT-HN) with 5′-triphosphate were produced by *in vitro* transcription. As shown in **Supplementary Figure S4**, the IVT-RNA secondary structures were predicted according to the RNA sequences. IVT-B2 had a nearly inverted repeat sequence at each end, which formed a secondary structure with a dsRNA terminus and an ssRNA loop; the IVT-HN sequence, which was from part of the Z strain HVJ *HN* gene, had no specific secondary structure. In **Figure 4a**, both IVT-B2 and IVT-HN were the same size as the viral DI RNA genome of the Cantell strain HVJ (βPL-Can-total). When the IVT-HN control RNA was transfected into PC3 cells using the same amount as with the IVT-B2 transfection, the cell death was not significantly up-regulated compared with the liposome only control (**Figure 4b**). In contrast, the transfection of IVT-B2 into the PC3 cells resulted in significant induction of cell death (**Figure 4b**), but IVT-B2 had no impact on cell viability in PNT2 cells, human keratinocyte cell line, and bovine aortic endothelial cell line (**Figure 5a** and **Supplementary Figure S5**). RIG-I/MAVS-related downstream proapoptotic protein expression was evaluated in the PC3 cells transfected with the IVT RNAs or HVJ RNAs (**Figure 4c**). TRAIL, Noxa, and the active form of caspase-3 were significantly upregulated in IVT-B2-transfected PC3 cells compared with the IVT-HN-transfected cells, a similar result was observed in MDA-MB-231 and A549 cells (**Supplementary Figure S6**). As shown in **Figure 4d**, the IVT-B2-induced expression of TRAIL, Noxa, the active form of caspase-3, and IFN-β was attenuated by the transfection of RIG-I siRNA. These results indicated that the IVT-B2 RNA, which was derived from the HVJ copy-back DI sequence, induced proapoptotic proteins expression in prostate cancer cells through the RIG-I pathway.

In addition, whether IVT-B2 RNA triggers chemoattraction and immunostimulation was examined in dendritic cells. After the transfection of IVT-B2 or IVT-HN into murine bone marrow dendritic cells (BM-DCs), the secretion of IFN-β and CXCL10 was evaluated. As illustrated in **Figure 4e**, the secretion of both IFN-β and CXCL10 were significantly increased in the IVT-B2-transfected BM-DCs compared with the IVT-HN-transfected cells. These results suggested that IVT-B2 RNA had the potential to promote chemoattraction and immunostimulatory capabilities of BM-DCs as previously reported using HVJ-E.[9] Next, we analyzed the RNA structure required for cancer-cell killing.

The double-stranded stem region of IVT-B2 was essential for selective cytotoxicity to cancer cells

HVJ DI-derived IVT RNA was modified to generate smaller sized IVT RNAs, IVT-R6 and IVT-L2, by deleting 3′ (nucleotides 95–272) or 5′ (nucleotides 273–450) portions of the ssRNA region in IVT-B2 (**Supplementary Figure S4**). The IVT-R6 and IVT-L2 RNAs transfection also resulted in the selective cancer cell killing effect (**Figure 5a**); additionally, RIG-I-dependent IFN-β secretion was stimulated by transfecting IVT-R6 and IVT-L2 into PC3 cells (**Figure 5b**). On the other hand, IVT-SB26 and IVT-SB17 with shorter dsRNA regions (26 bp and 17bp long) and the identical ssRNA loop region of IVT-B2 (**Supplementary Figure S4**) were constructed and synthesized *in vitro*. As shown in **Figure 5c**,d, IVT-SB17 had no activity of cancer cell killing and hardly upregulated the expression of proapoptotic genes such as *Noxa* and *TRAIL*. Transfection of IVT-SB26 showed a partial response in the induction of cancer cell death and proapoptotic proteins expression compared with IVT-B2.

The 5′-triphosphate of RNA plays a role in the recognition of pathogenic RNA genomes by RIG-I.[25] We confirmed that calf intestinal alkaline phosphatase (CIAP)-treated IVT-B2 RNA lost the capability of inducing RIG-I/MAVS-related downstream Noxa and TRAIL expression (**Supplementary Figure S7a**) and IFN-β secretion in PC3 cells (**Supplementary Figure S7b**). These results suggested that both the double-stranded stem region and 5′-triphosphate of IVT-B2 are crucial in inducing the RIG-I/MAVS-related downstream anticancer effects. In addition, we investigated whether the structure of HVJ-E RNA fragments are responsible for RIG-I-mediated IFN-β secretion. When total Z-HVJ-E RNA fragments were transfected to PC3 cells, IFN-β was produced in a dose-dependent manner, but with CIAP treatment, no IFN-β was detected (**Supplementary Figure S8a**). This suggests that a part of UV-irradiated Z-HVJ-E RNA fragments had 5′-triphosphates. Since, theoretically, the 5′ terminal sequence should have 5′-triphosphate, the RNA secondary structure of 5′ terminal sequence of Z strain HVJ genome (nucleotides 1–544) was predicted by CentroidFold. As shown in **Supplementary Figure S8b**, the RNA was estimated to have double-strand stems (18, 24, and 36 bp long) in the 5′ terminal sequence of HVJ genome. The *in vitro* transcribed 5′ terminal 544 base RNA (IVT-Z544) induced RIG-I dependent IFN-β secretion in PC3 cells (**Supplementary Figure S8c**).

IVT-B2 suppressed PC3 xenograft tumors and induced intratumoral apoptosis in immunodeficient mice

To demonstrate the *in vivo* anticancer effect of IVT-B2, a xenograft prostate cancer model in immunodeficient CB.17-SCID mice was established. IVT-B2 or IVT-HN RNA was intratumorally transfected into xenograft PC3 tumors via *in vivo* electroporation. As depicted in **Figure 6a**, the IVT-B2-transfected xenograft PC3 tumors expressed higher levels of TRAIL than the IVT-HN-transfected tumors. A significant increase in terminal deoxynucleotidyl transferase dUTP nick-end labeling (TUNEL)-positive apoptotic cells was detected in the IVT-B2-transfected PC3 tumor (**Figure 6b**). The PC3 tumor growth was extensively suppressed by three doses of IVT-B2 RNA (**Figure 6c**). Thus, the

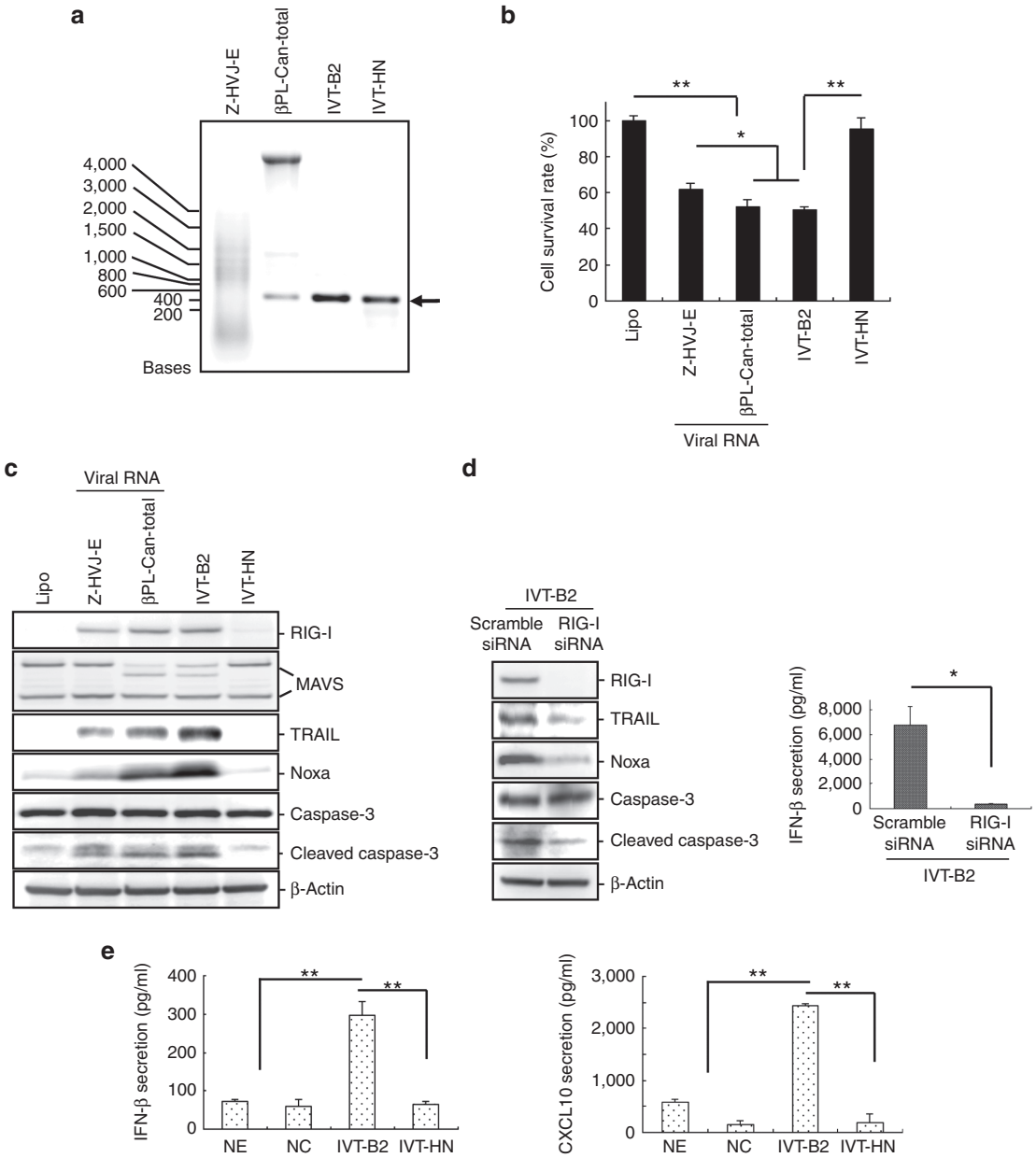

Figure 4 IVT-DI RNA induced cancer cell death and apoptosis-related proteins expression in PC3 cells. (**a**) The IVT RNAs, RNA of Z-HVJ-E or RNA of βPL-Can-total were separated by RNase-free agarose gel electrophoresis. The arrow indicates the size of the DI genome RNA. (**b**) The HVJ RNAs or IVT RNAs (1.16 ng/ml) were transfected into PC3 cells, and the cell survival was detected by MTS assay 48 hours after RNA transfection. (**c**) Expression levels of RIG-I, MAVS, TRAIL, Noxa, and caspase 3 were measured by western blot analysis 24 hours after HVJ RNAs or IVT-RNAs transfection into PC3 cells. (**d**) IVT-B2 RNA (1.16 ng/ml) was transfected into RIG-I-knocked-down PC3 cells (RIG-I siRNA-transfected) or control PC3 cells (scramble siRNA-transfected). RIG-I, TRAIL, Noxa, and caspase-3 expression levels (left panel) and IFN-β secretion (right panel) were assessed 24 or 48 hours after IVT-B2 RNA transfection. (**e**) IVT-B2 or IVT-HN RNA was transfected into bone marrow-derived dendritic cells (BM-DCs) by *in vitro* electroporation. IFN-β (left panel) and CXCL10 (right panel) secretions in culture medium were assessed using an ELISA 24 hours after IVT RNAs transfection. "NE" indicates BM-DCs that were treated with IVT-B2 but without the electroporation process. "NC" indicates BM-DCs that were subjected to electroporation without RNA. The mean ± SD is shown ($n = 3$). *$P < 0.05$; **$P < 0.01$. ELISA, enzyme-linked immunosorbent assay. MTS, 3-(4,5-dimethyl-2-yl)-5-(3-carboxymethoxyphenyl)-2-(4-sulfophenyl)-2H-tetrazolium, inner salt.

in vivo induction of intratumoral apoptosis and tumor suppression by IVT-B2 RNA in an immunodeficient mouse model were confirmed.

Furthermore, the immunostimulatory capacity of IVT-B2 *in vivo* was also investigated to confirm the involvement of NK cells in the IVT-B2-induced *in vivo* anticancer effect. To deplete NK cell activity, anti-asialo-GM1 antibodies were administered to CB.17-SCID mice via i.p. injections. As shown in **Figure 6d**, in the control IgG antibody-treated CB.17-SCID mice, intratumoral transfection of IVT-B2 decreased the PC3 tumor volume; in contrast, the IVT-B2-induced tumor suppression was significantly impaired by anti-asialo-GM1 antibody treatment. This result suggested that IVT-B2 RNA was effective in inducing anticancer NK activity *in vivo* in an immunodeficient mouse model.

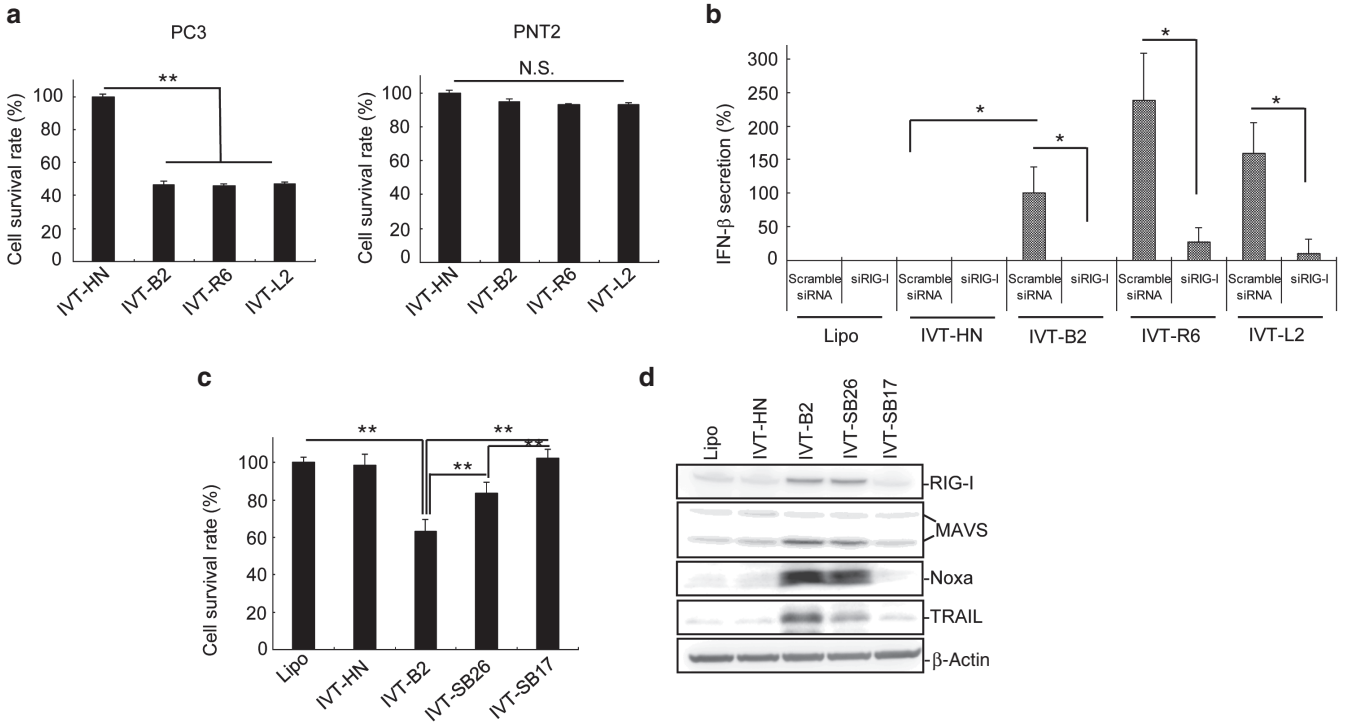

Figure 5 The double-stranded stem region of IVT-B2 is essential for selective cytotoxicity to cancer cells. (**a**) PC3 and PNT2 cell survival rates were detected 48 hours after IVT-RNAs (1.16 ng/ml) transfection with MTS assay. (**b**) IVT-RNAs was transfected into RIG-I-knocked-down PC3 cells (RIG-I siRNA-transfected) or control PC3 cells (scramble siRNA-transfected). IFN-β secretion was assessed 48 hours after IVT-B2 RNA transfection. "Lipo" indicates cells that were treated with Lipofectamine RNAiMAX without RNA. (**c**) PC3 cell survival rates were detected 48 hours after IVT-RNAs transfection with MTS assay. The mean ± SD is shown ($n = 3$). *$P < 0.05$; **$P < 0.01$. ($n = 3$). (**d**) Expression levels of RIG-I, MAVS, TRAIL, and Noxa were analyzed by western blot 24 hours after IVT-RNAs transfection into PC3 cells. MTS, 3-(4,5-dimethyl-2-yl)-5-(3-carboxymethoxyphenyl)-2-(4-sulfophenyl)-2H-tetrazolium, inner salt.

DISCUSSION

In this study, we demonstrated that HVJ DI particle-derived IVT-DI RNA induced cancer cell apoptosis through RIG-I downstream signaling. In previous studies, viral replication was essential in most of the oncolytic virotherapies.[7] However, in our recent studies, the UV-irradiated HVJ-E without viral replication activity exhibited anticancer effects through the induction of anticancer immunity and oncolysis.[8,26] Previous studies demonstrated that HVJ encoded C proteins counteracting the antiviral action of IFNs.[27,28] The apoptosis of HVJ-infected cells were prevented by C-protein presence through inhibition of signal transducer and activator of transcription.[27,29] Cancer cell killing activity of live Z strain HVJ is less than that of inactivated HVJ-E presumably due to the expression of C protein in live HVJ-infected cells.[12] The HVJ-E genomic RNA fragments promoted cancer cell apoptosis by triggering RIG-I/MAVS signaling and inducing the downstream expression of Noxa and TRAIL. It has been reported that RIG-I preferentially recognizes shorter dsRNA (~300 bp to 1 kb).[16] The UV-irradiated Z-HVJ-E RNA was a mixture that had RNA fragments of various sizes (100–8,000 nucleotides) (**Figure 1a**); the viral RNA fragments with shorter sizes might be the primary inducers of RIG-I-dependent apoptosis. HVJ Cantell strain-derived DI particles include a smaller sized RNA genome with ~550 nucleotides, and it is reported that the DI RNA genome is a strong inducer of RIG-I downstream type-I IFN expression in DCs.[15] Similarly, βPL-Cantell-HVJ without viral replication activity can induce RIG-I-related proapoptotic proteins expression in cancer cells (to even higher levels than UV-irradiated Z-HVJ-E) (**Figure 1d**). The RNA from the DI-rich fraction of βPL-Cantell-HVJ was able to induce more Noxa expression in both the PC3 and DU145 hormone-resistant human prostate cancer cell lines but not in noncancerous PNT2 cells (**Figure 2c**). Moreover, it was confirmed that gel-extracted DI RNA promoted cancer cell death more effectively than the gel-extracted HVJ genomic RNA. Although the gel-extracted HVJ genomic RNA had a fractional effect on the induction of apoptosis in PC3 cells, the DI RNA was likely the main source of the RIG-I-dependent cancer cell death (**Figure 3**). Z HVJ-E- or βPL-Cantell HVJ-treated PC3 cells secreted IFN-β. In contrast, MDA-MB-231 cells did not secret IFN-β but transfection with the gel-extracted DI RNA induced a significant cell death in MDA-MB-231 cells (**Supplementary Figure S3**), as did treatment with HVJ-E or βPL-Cantell HVJ; this result was also observed with DU145 cells (data not shown). It is suggested that IFN-β secretion in cancer cells magnifies the viral RNA-induced cancer cell death, although this relationship is not indispensable for leading to apoptosis. The direct induction of cancer cell apoptosis was attributed to the DI RNA.

Either reovirus infection or the transfection of segments of the reovirus genome stimulates RIG-I-dependent type-I IFN production in cells.[16,30] Through studying reovirus, it was clarified that the viral RNA with 5′-diphosphate is sufficient to trigger the IFN-β promoter, whereas RNA with 5′-triphosphate more effectively augments the production of type-I IFNs through

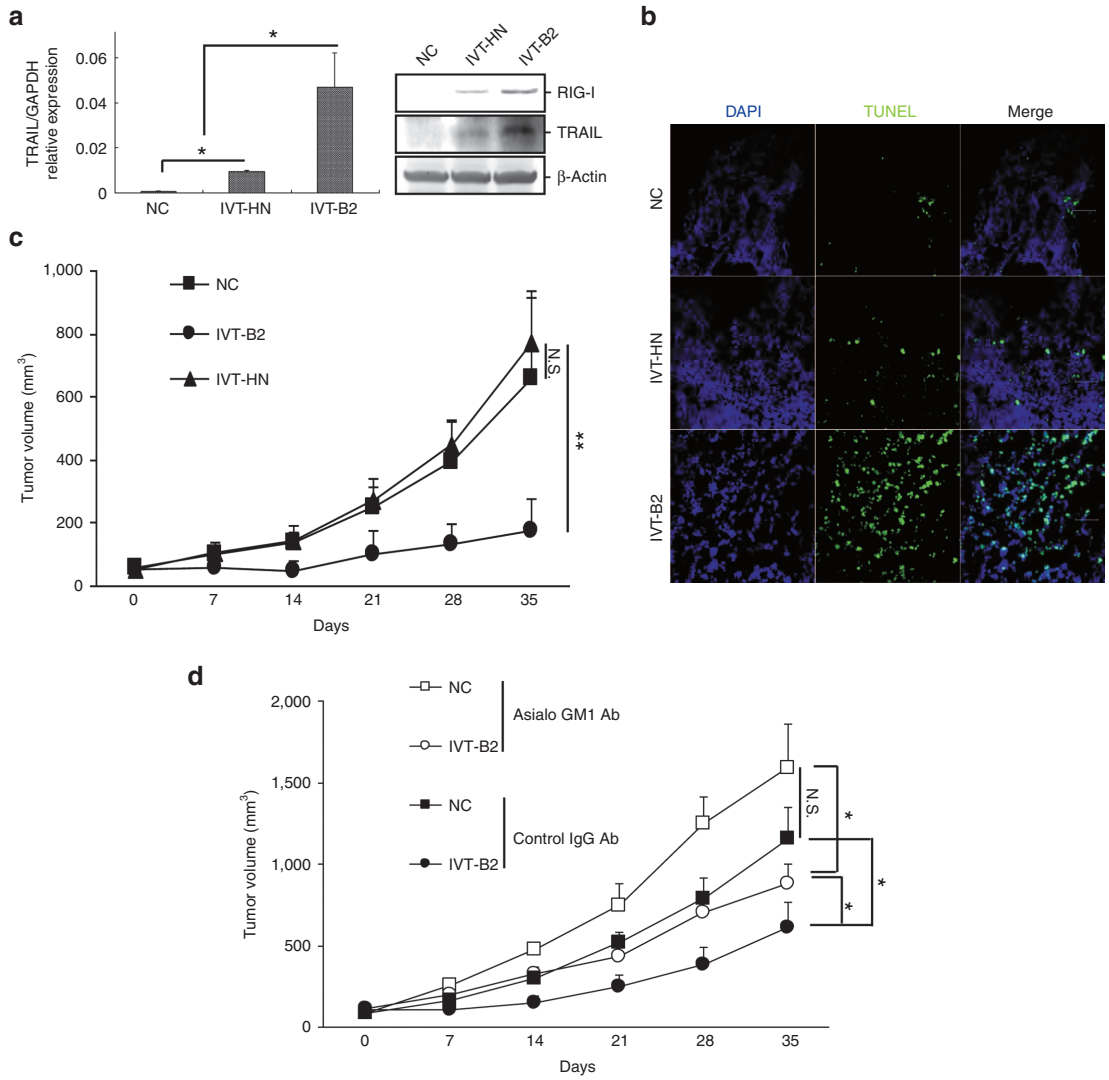

Figure 6 Transfection of IVT-B2 RNA by *in vivo* electroporation suppressed PC3 xenograft tumor and induced intratumoral apoptosis in immunodeficient mice. A total of 5 μg of IVT-B2, IVT-HN RNA, or ddH_2O only (NC) was transfected into PC3 xenograft tumors by *in vivo* electroporation in CB-17/SCID mice. (**a**) The expression levels of RIG-I and TRAIL were evaluated by western blot analysis (right panel), and the transcription of TRAIL was evaluated by real-time quantitative PCR in PC3 xenograft tumors 48 hours after IVT-RNAs transfection (left panel). IVT-B2 ($n = 3$), IVT-HN ($n = 3$), and NC groups ($n = 3$). (**b**) The apoptotic cells in the PC3 xenograft tumors were evaluated by TUNEL staining 48 hours after transfection with the IVT RNAs. Bar = 100 μm. (**c**) PC3 xenograft tumor volumes were evaluated. The IVT-RNAs were transfected on days 0, 3, and 6 by *in vivo* electroporation in the IVT-B2 ($n = 7$), IVT-HN ($n = 8$), and NC groups ($n = 7$). $^{**}P < 0.01$. (**d**) IVT-RNAs or ddH_2O only (NC) were transfected to PC3 xenograft tumor by *in vivo* electroporation in CB-17/SCID mice, which were treated with NK cell-depletion using anti-asialo GM1 antibodies or control IgG antibodies. Tumor volumes are shown (mean ± SD) for the IVT-B2 ($n = 4$), IVT-HN ($n = 4$), and NC group ($n = 3$). N.S., no significant difference. $^{*}P < 0.05$.

RIG-I recognition.[31] Our study proved that the 5′-triphosphate in the HVJ-derived IVT-DI RNA was also crucial in the induction of IFN-β secretion from PC3 cells; moreover, the presence of 5′-triphosphate in the IVT-DI RNA was positively correlated with the RIG-I-dependent expression of Noxa and TRAIL in prostate cancer cells (**Supplementary Figure S7a**). Moreover, previous studies have shown that RIG-I is activated by both 5′-triphosphate dsRNA and ssRNA.[17] In this study, IVT-R6 and IVT-L2 (**Figure 5a**) with shorter ssRNA regions and an identical dsRNA stem region of IVT-B2 were constructed to determine the effective part of the DI RNA fragment. IFN-β secretion and cancer cell-specific apoptosis were not affected by losing the 3′ or 5′ terminal ssRNA region of the IVT-DI RNA (**Figure 5a**,b). The dsRNA stem region of the IVT-DI RNA could be the most important part in triggering the RIG-I-related anticancer effect, whereas IVT-HN with 5′-triphosphate failed to induce cancer cell apoptosis. Previous study reported that a 25 bp chemically synthesized dsRNA (siRNA) with blunt end induces the expression of IFN-induced protein with tetratricopeptide repeats 1 (IFT1/P56) in human fibroblast cells.[32] In our study, IVT-SB26 transfection induced PC3 cell death, but the effect was less than IVT-B2 while no cell killing was seen with IVT-SB17 (**Figure 5c**,d). It is likely that the minimal length of the dsRNA stem of HVJ DI-derived IVT-RNA required for RIG-I downstream cancer cell death is between 17 and 26 bp. Taken together, both the double-stranded stem and presence of 5′-triphosphate in the DI RNA are essential for the induction of cancer cell-specific apoptosis.

Our prior studies have demonstrated that HVJ-E induced the secretion of CXCL10 in DCs.[9] CXCL10 contributes to the

chemoattraction of NK cells, monocytes/macrophages, T cells, and DCs.[33,34] In this study, IVT-B2 transfection induced CXCL10 and IFN-β secretion in BM-DCs. The involvement of NK cells in the IVT-B2 RNA-induced anticancer effects were proved in an NK cell-depleted immunodeficient mouse that was transplanted with human PC3 cancer cells (**Figure 6d**). Taken together, our findings suggest that after the administration of IVT-B2 RNA, active NK cells may be attracted to the tumor by CXCL10, and the IFN-β may enhance NK cell activity in the tumor microenvironment.

In our study, a small amount (0.067 or 1.16 ng/ml) of isolated viral RNA or IVT-DI RNAs induced cancer cell death and RIG-I-related apoptotic proteins expression, whereas treatment with UV-irradiated HVJ-E or inactivated βPL-HVJ required more than a hundred times that amount of viral RNA. Moreover, DI-RNA induced apoptosis in cancer cells but not in noncancerous cells and suppressed the growth of xenograft tumors *in vivo*. DI particles of Cantell strain HVJ contribute to the TLR-independent immunostimulatory ability.[15] Antitumor effect may be enhanced by combination of DI-RNA or similar reagents that induce RIG-related anticancer effect with other therapeutic drugs such as Toll-like receptor agonists.

Through studying the DI genome of the Sendai virus, the RNA characteristics that induce cancer cell-selective apoptosis were clarified. Significant tumor-suppressive effects caused by copy-back DI genomic RNA were demonstrated. In addition, a large amount of IVT-DI RNA could be efficiently produced *in vitro*. Therefore, these findings provide an alternative way to develop a novel nucleic acid medicine for the treatment of cancer and infectious diseases.

MATERIALS AND METHODS

Cells and mice. The hormone-resistant human prostate cancer cell lines PC3 and DU145, the A549 human lung cancer cell line, the MDA-MB-231 human breast cancer cell line, immortalized human epidermal keratinocyte, and bovine aortic endothelial cells were purchased from the American Type Culture Collection (ATCC, Manassas, VA). The human normal prostate epithelial cell line PNT2 was purchased from the European Collection of Animal Cell Cultures (Salisbury, UK). The cell lines were maintained in Dulbecco's modified Eagle's medium (Nacalai Tesque, Kyoto, Japan), with 10% fetal bovine serum (Biowest, Nuaillé, France), 100 U/ml penicillin, and 100 mg/ml streptomycin (penicillin–streptomycin mixed solution; Nacalai Tesque, Kyoto, Japan). Mouse splenocytes and murine BM-DCs were isolated from C57BL/6N mice. The BM-DCs were generated as previously described.[9] All of the cells were incubated at 37 °C in a humidified atmosphere of 95% air and 5% CO_2.

Severe combined immunodeficient (C.B-17 SCID) mice, aged 8 weeks, and C57BL/6N mice, aged 6–8 weeks, were purchased from Clea Japan (Tokyo, Japan) and were maintained in a temperature-controlled, pathogen-free room. All of the animals were handled according to the approved protocols and guidelines of the Animal Committee of Osaka University (Osaka, Japan).

Preparation of inactivated HVJs. The Z strain of HVJ (VR-105 parainfluenza 1 Sendai/52 strain from the ATCC) was amplified in the chorioallantoic fluid of 10- to 14-day-old chick eggs. The Z-HVJ viral particles were then purified by centrifugation from the chorioallantoic fluid. The purified viruses were inactivated by UV irradiation (99 mJ/cm^2), as previously described.[35]

The βPL-Noe-Z and βPL-Cantell HVJ were purchased from Ishihara Sangyo, (Osaka, Japan). βPL-Noe-Z-HVJ was obtained from GenomONE-Neo Transfection Reagent (GN001). βPL-Cantell-HVJ was from GenomONE Transfection Reagent (GE001). In these Transfection Kits, the viral replication activity in both βPL-Noe-Z-HVJ and βPL-Cantell-HVJ were inactivated by βPL.

Preparation of the inactivated HVJ RNAs. Inactivated Cantell strain HVJ (VR-907 parainfluenza 1 Cantell, Cantell strain from the ATCC) was amplified by the same protocol as the Z strain HVJ described above. Instead of UV irradiation, the chorioallantoic fluid that contained Cantell strain HVJ was treated with 0.008% β-propiolactone for 1 hour at room temperature to inactivate the viral replication. The supernatant of the chorioallantoic fluid was retained after the purification by centrifugation of the inactivated Cantell strain HVJ. Thus, the Cantell strain HVJ DI particle-rich fraction was generated from the supernatant of the chorioallantoic fluid by high-speed centrifugation (~73,000 × *g*, 75 minutes, 4 °C).

The inactivated-HVJ RNAs were isolated from UV-irradiated Z stain HVJ (Z-HVJ-E), βPL-treated Cantell strain HVJ (Can-total), or Cantell strain HVJ DI particle-rich fraction (Can-DI-rich) with ISOGEN (311–02501; Nippon Gene, Toyama, Japan).

Preparation of agarose gel-extracted Cantell strain RNA. The ISOGEN-isolated Cantell HVJ RNA was separated into the Cantell HVJ whole-genome RNA and Cantell HVJ DI genome RNA fractions using an RNase-free electrophoresis agarose gel kit (N726-KIT; Amresco, Solon, OH) and SeaKem GCG Agarose (50070; Cambrex Bio Science Rockland, Rockland, ME). The RNA fractions were extracted with thermostable β-Agarase (311-07121; Nippon Gene) and ISOGEN.

IVT RNAs. IVT RNA was produced using the T7 Quick High Yield RNA synthesis Kit (E2050S; New England BioLabs, Ipswich, MA) according to the manufacturer's instructions. The RNeasy mini kit (74106; Qiagen, Hilden, Germany) was used to clean up the produced IVT RNAs. A template plasmid that expressed IVT-B2 RNA was constructed by PCR amplification of the Cantell HVJ DI genome sequence of Cantell HVJ-infected A549 cells. The template plasmids that expressed IVT-HN and IVT-Z544 RNAs were constructed from the Z strain HVJ *HN* gene mRNA sequence and *L* gene sequence, respectively, by the protocol described above. Template plasmids that expressed IVT-R6, IVT-L2, IVT-SB26, and IVT-SB17 RNAs were produced from the IVT-B2 plasmid by PCR amplification and the In-Fusion HD Cloning Kit (63964; Clontech Laboratories, Tokyo, Japan). The DNA template sequences of the IVT RNA plasmids were confirmed by Sanger dideoxy chain termination sequencing analysis, and the fluorescent bases were detected with a 3100 Genetic Analyzer (Applied Biosystems, Waltham, MA).

The template DNA sequences for the IVT RNAs were as follows:

IVT-B2: taatacgactcactataACCAGACAAGAGTTTAAGAGATATCC
ATTCTTCCAAATTTTCTTGTCTCCCTGCAAGTTCCACTTACC
ATTGTCATATGGACAAGTCCAAGACTTCCAGGTACCGCGG
AGCTTCGATCGTTCTGCACGACAGGGACTAATTATTACGAGCT
GTCATATGGCTCGATATCACCCAGTGATCCATCATCAATCACG
GTCGTGTATTCATTCTGCCTGGCCCCGAACATCCTGACCG
CCCCTAAAATCTTCATCAAAATCTTCATTTCTTTGGTGAG
GAATCCATACGTTATACTATGTATAATCCTCAAACCTGTCC
AATAAAGTTTTTGTGATAACCCTCAGGTTCCTGATCTCACG
GGATGACAATGAAACCACTCCCAATTGAAGTCTTGCCTC
AAACTTCTGGTCAGGGAATGACCCAGCCACCAATCCTGTGG
ACATAGATAAAGATAGTCTTGGACTTATCCACATGACAACAGC
AAGAAAAACTCACAAGAAGACAAGAAAATTCAAAAGAATC
AATATCTCCCAAACTCTTGTCTGGT

IVT-HN: taatacgactcactataGGGTGATACAAAATGTAGGACCCAA
GGATGCCAACAGGTGTCGCAAGACACATGCAATGAGGCTCTG
AAAATTACATGGCTAGGAGGGAAACAGGTGGTCAGCGTGATC
ATCCAGGTCAATGACTATCTCTCAGAGAGGCCAAAGATAA
GAGTCACAACCATTCCAATCACTGAAAACTATCTCGGGGCGG
AAGGTAGATTATTAAAATTGGGTGATCGGGTGTACATCTATAC
AAGATCATCAGGCTGGCACTCTCAACTGCAGATAGGAGTACTTG

ATGTCAGCCACCCTTTGACTATCAACTGGACACCTCATG
AAGCCTTGTCTAGACCAGGAAATAAAGAGTGCAATTGGTAC
AATAAGTGTCCGAAGGAATGCATATCAGGCGTATACACTGATG
CTTATCCATTGTCCCCTGATGCAGCTAACGTCGCTACCGTC
ACGCTATATGCCAATACATCGCGTGTCAACCCAACAATCATGT
ATTCTAACACTACTAACATTATAAATATGTTAAGGATAAAGGATG
TTCAATTAGAGGCT

IVT-L2: taatacgactcactataACCAGACAAGAGTTTAAGAGATATCC
ATTCTTCCAAATTTTCTTGTCTCCCTGCAAGTTCCACTTACC
ATTGTCATATGGACAAGTCCAAGACTTCCAGGTACCGCGG
AGCTTCGATCGTTCTGCACGACAGGGACTAATTATTAC
GAGCTGTCATATGGCTCGATATCACCCAGTGATCCATCATC
AATCACGGTCGTGTATTCATTCTGCCTGGCCCCGAACATCCTG
ACCGCCCCTAAAATCTTCATCAAAATCTTCATTTCTTTGG
TGAGTCTTGGACTTATCCACATGACAACAGCAAGAA
AAACTCACAAGAAGACAAGAAAATTCAAAAGAATC
AATATCTCCCAAACTCTTGTCTGGT

IVT-R6: taatacgactcactataACCAGACAAGAGTTTAAGAGATATC
CATTCTTCCAAATTTTCTTGTCTCCCTGCAAGTTCCACTTAC
CATTGTCATATGGACAAGTCCAAGACTAGGAATCCATACGTT
ATACTATGTATAATCCTCAAACCTGTCCAATAAAGTTTTTGTG
ATAACCCTCAGGTTCCTGATCTCACGGGATGACAATGAAACC
ACTCCCAATTGAAGTCTTGCCTCAAACTTCTGGTCAGGGAAT
GACCCAGCCACCAATCCTGTGGACATAGATAAAGATAGTCTTG
GACTTATCCACATGACAACAGCAAGAAAAACTCACAAGAAGAC
AAGAAAATTCAAAAGAATCAATATCTCCCAAACTCTTGTCTGGT

IVT-SB26:

taatacgactcactataGTTGTCATATGGACAAGTCCAAGACTTCC
AGGTACCGCGGAGCTTCGATCGTTCTGCACGACAGGGACT
AATTATTACGAGCTGTCATATGGCTCGATATCACCCAGTG
ATCCATCATCAATCACGGTCGTGTATTCATTCTGCCTGG
CCCCGAACATCCTGACCGCCCCTAAAATCTTCATC
AAAATCTTCATTTCTTTGGTGAGGAATCCATACGTTATACT
ATGTATAATCCTCAAACCTGTCCAATAAAGTTTTTGTGATAA
CCCTCAGGTTCCTGATCTCACGGGATGACAATGAAACC
ACTCCCAATTGAAGTCTTGCCTCAAACTTCTGGTCAGGGAATG
ACCCAGCCACCAATCCTGTGGACATAGATAAAGATAGTCTTGG
ACTTATCCACATGACAAC

IVT-SB17:

taatacgactcactataTGGACAAGTCCAAGACTTCCAGGTACC
GCGGAGCTTCGATCGTTCTGCACGACAGGGACTAATTATT
ACGAGCTGTCATATGGCTCGATATCACCCAGTGATCCATCATC
AATCACGGTCGTGTATTCATTCTGCCTGGCCCCGAACATCCTG
ACCGCCCCTAAAATCTTCATCAAAATCTTCATTTCTTTGGTG
AGGAATCCATACGTTATACTATGTATAATCCTCAAACCTGTCC
AATAAAGTTTTTGTGATAACCCTCAGGTTCCTGATCTCACG
GGATGACAATGAAACCACTCCCAATTGAAGTCTTGCCTC
AAACTTCTGGTCAGGGAATGACCCAGCCACCAATCCTGTGGAC
ATAGATAAAGATAGTCTTGGACTTATCCA

IVT-Z544:

taatacgactcactataACCAGACAAGAGTTTAAGAGATATGT
ATTCTTTTAAATTTTCTTGTCTTCTTGTAAGTTTTTCTTACT
ATTGTCATATGGATAAGTCCAAGACTTCCAGGTACCGCGG
AGCTTCGATCGTTCTGCACGATAGGGACTAATTATTACGAGCTG
TCATATGGCTCGATATCACCTAGTGATCCATCATCAATCACG
GTCGTGTATTCATTTTGCCTGGCCCCGAACATCTTGACTG
CCCCTAAAATCTTCATCAAAATCTTTATTTCTTTGGTGAGG
AATCTATACGTTATACTATGTATAATATCCTCAAACCTGTCT
AATAAAGTTTTTGTGATAACCCTCAGGTTCCTGATCTC
ACGGGATGATAATGAAACTATTCCCAATTGAAGTCTTG
CTTCAAACTTCTGGTCAGGGAATGACCCAGTTACCAATCTTG
TGGACATAGATAAAGATATCCAAGATAGCACAAGTCTTCT
AGAAATTGTCTTCAACTTGCCTGAATCTCTCACAGGATACAGG
TCATACTTACCAGTTAGTTTGAGCCT

The sequence of the T7 promotor is shown in lowercase letters, and the sequence of transcript RNA is shown in capital letters.

Transfection of the HVJ RNAs and IVT RNAs into cells. HVJ-E RNAs or IVT RNAs were transfected into cancer cells by using Lipofectamine RNAiMAX reagent (Invitrogen, Waltham, MA). The IVT RNA concentration was 0.067 or 1.16 ng/ml. The medium was changed to Dulbecco's modified Eagle's medium 5 hours after the RNA transfection. IVT RNAs (2.18 ng/ml) were transfected into BM-DCs (2×10^5 cells) with an *in vitro* electroporation kit, Neon Transfection System kit (MPK5000; Invitrogen).

Evaluation of IFN-β and CXCL10 secretion levels in cell culture medium. The secretion of IFN-β by mouse splenocytes and BM-DCs was evaluated by a VeriKine Mouse IFN-β ELISA Kit (42400; pbl interferon source, Piscataway, NJ) in cell culture medium. The secretion of CXCL10 by BM-DCs was evaluated using the VeriKine Mouse CXCL10 Quantikine ELISA Kit (MCX100; R&D Systems, Minneapolis, MN) in culture medium 24 hours after transfection with IVT RNAs. The IFN-β secretion of cancer cell lines was evaluated by a VeriKine Human IFN-β ELISA Kit (41410; pbl interferon source) in cell culture medium.

Preparation of CIAP-treated IVT RNA. The 5′-phosphate groups of IVT-B2 RNA or HVJ-E RNA were hydrolyzed using a calf intestinal alkaline phosphatase kit (18009–019; Invitrogen). IVT-B2 RNA or HVJ-E RNA was treated with CIAP (0–1 U/μg or 1 U/μg) for 30 minutes at 37 °C. After CIAP hydrolyzation, the CIAP-treated RNA was extracted with an RNeasy mini kit (74106; Qiagen).

Antibodies and western blotting. The anti-MAVS antibody (ab25084) and anti-Noxa antibody (ab13654) were purchased from Abcam, while the anti-TRAIL (C92B9) antibody (#3219) and the anti-caspase-3 antibody (#9662S) were purchased from Cell Signaling (Danvers, MA). Anti-RIG-I (C-15) antibody (sc-48929) was purchased from Santa Cruz Biotechnology (Dallas, TX). The anti-β-actin (AC-15) antibody (A5441) was purchased from Sigma-Aldrich Japan (Tokyo, Japan). The cell lysates were separated by 10–20% gradient polyacrylamide gel electrophoresis and transferred onto polyvinylidene difluoride membranes. Signals were detected with Chemi-Lumi one (Nacalai Tesque Kyoto, Japan) and ImmunoStar LD (290–69904; Wako Pure Chemical Industries, Osaka, Japan) following the manufacturer's instructions.

RIG-I siRNA transfection into cells. RIG-I siRNA (DDX58-HSS177513; Invitrogen) and scrambled siRNA (46–2001, Negative control medium GC; Invitrogen) were transfected into cells with Lipofectamine RNAiMAX reagent (Invitrogen) following the manufacturer's protocol. The concentration of siRNA was 100 pmol/well.

3-(4,5-dimethyl-2-yl)-5-(3-carboxymethoxyphenyl)-2-(4-sulfophenyl)-2H-tetrazolium, inner salt (MTS) cell proliferation assay. A CellTiter 96 AQueous One Solution Cell Proliferation Assay Kit (Promega) was used to evaluate the cell survival. After transfection with the HVJ-E RNA or IVT RNAs, 100 μl of CellTiter 96 Aqueous One Solution was added to 1 ml of medium. The absorbance at 490 nm was measured in each well with a 96-well Mithras LB 940 Multimode Microplate Reader (Berthold Technologies, Bad Wildbad, Germany).

Treatment with IVT-B2 RNA in a prostate cancer xenograft tumor mouse model. A PC3 xenograft tumor was established on the back of immunodeficient mice (C.B-17 SCID, female, 8 weeks old) by intradermal injection with 5×10^6 cells/50 μl phosphate-buffered saline per mouse. IVT RNA was transfected in the xenograft PC3 tumor on days 0, 3, and 6 via *in vivo* electroporation. In each treatment, 5 μg of IVT-B2 or IVT-HN RNA in a volume of 50 μl double-distilled water (ddH_2O) was injected intratumorally. Then, the IVT-RNA-injected PC3 tumor was treated with *in vivo* electroporation by a 5-mm diameter electrode (CUY650-5; Nepa Gene, Chiba, Japan)

and Electro Square Porator (ECM830; BTX Harvard Apparatus, Holliston, MA). The *in vivo* electroporation parameters were five square pulses of 50-ms duration and 70 V. The tumor volumes were calculated according to the following formula: tumor volume (mm^3) = length × $(width)^2/2$.

Treatment with IVT-B2 RNA of NK cell-depleted model mice bearing a prostate cancer xenograft tumor. PC3-tumor-bearing mice (C.B-17 SCID, female, 8 weeks old) were treated with antiasialo GM1 antibody (014-09801; Wako Pure Chemical industries) for NK cell depletion or control IgG antibody (IgG from rabbit serum, I5006; Sigma-Aldrich Japan) by i.p. injection on days −1, 0, 1, 2, 4, 6, 9, and 12. The IVT RNA was transfected in the xenograft PC3 tumor on days 0, 3, and 6 by *in vivo* electroporation, as described above.

TUNEL assay. A PC3 xenograft tumor was established on the back of immunodeficient mice (C.B-17 SCID, female, 8–10 weeks old); 5 μg of IVT-B2, IVT-HN RNA, or ddH_2O was transfected into the xenograft PC3 tumor by *in vivo* electroporation. The apoptotic cells in the PC3 xenograft tumors were evaluated using the DeadEnd™ Fluorometric TUNEL System (TB235, Promega, Madison, WI) 48 hours after transfection with the IVT RNAs.

RNA extraction and quantification. A PC3 xenograft tumor was established on the back of immunodeficient mice (C.B-17 SCID, female, 8–10 weeks old); 5 μg of IVT-B2, IVT-HN RNA, or ddH_2O (NC) was transfected into the xenograft PC3 tumor by *in vivo* electroporation. RNA was extracted from PC3 xenograft tumor with ISOGEN, 48 hours after transfection with the IVT RNAs. One microgram of total RNA was converted to cDNA with the High-Capacity cDNA Reverse Transcription Kit (Applied Biosystems, Waltham, MA). The human TRAIL and GAPDH were amplified by SYBR Premix Ex Taq (Takara Bio, Shiga, Japan). TRAIL and GAPDH primers (Hs00234356_m1, Hs99999905_m1; Thermo Fisher Scientific, Waltham, MA) were used. All procedures were carried out according to the manufacturer's instructions.

Statistical analyses. The results are reported as the mean ± SD. The statistical significance of differences between two groups was detected by a two-tailed unpaired Student's *t*-test. Differences were considered to be significant at the probability value (P) < 0.05.

SUPPLEMENTARY MATERIAL

Figure S1. Inactivated-Cantell strain HVJ stimulated IFN-β secretion in A549 cells.

Figure S2. The RNA amount of inactivated-HVJs.

Figure S3. Gel-extracted DI RNA was more efficient than Cantell strain HVJ whole-genome RNA for cancer cell killing and the induction of apoptosis-related proteins expression in MDA-MB-231 cells.

Figure S4. The secondary structure of IVT-RNAs.

Figure S5. Survival of non-cancerous cells by IVT-B2 transfection.

Figure S6. IVT-B2 RNA induced proapoptotic proteins expression in MDA-MB-231 and A549 cells.

Figure S7. Dephosphorylated IVT-B2 RNA lost the capability of inducing RIG-I/MAVS-related downstream proapoptotic proteins expression.

Figure S8. The *in vitro* transcription produced Z strain HVJ genome 5′ end RNA (IVT-Z544) induced RIG-I dependent IFN-β secretion in PC3 cells.

ACKNOWLEDGMENTS

This study was supported by the Japan Cancer Research grant from AMED (15ck0106127h0002), the program for the Promotion of Fundamental Studies in Health Sciences of the National Institute of Biomedical Innovation (Project ID: 10-03), and Grant-in-Aid for Scientific Research (B) from Japan Society for the Promotion of Science.

REFERENCES

1. DeSantis, CE, Lin, CC, Mariotto, AB, Siegel, RL, Stein, KD, Kramer, JL *et al.* (2014). Cancer treatment and survivorship statistics, 2014. *CA Cancer J Clin* **64**: 252–271.
2. Gregory, CW, He, B, Johnson, RT, Ford, OH, Mohler, JL, French, FS *et al.* (2001). A mechanism for androgen receptor-mediated prostate cancer recurrence after androgen deprivation therapy. *Cancer Res* **61**: 4315–4319.
3. Lorence, RM, Rood, PA and Kelley, KW (1988). Newcastle disease virus as an antineoplastic agent: induction of tumor necrosis factor-alpha and augmentation of its cytotoxicity. *J Natl Cancer Inst* **80**: 1305–1312.
4. Coffey, MC, Strong, JE, Forsyth, PA and Lee, PW (1998). Reovirus therapy of tumors with activated Ras pathway. *Science* **282**: 1332–1334.
5. Saga, K and Kaneda, Y (2013). Virosome presents multimodel cancer therapy without viral replication. *Biomed Res Int* **2013**: 764706.
6. Kirn, D, Martuza, RL and Zwiebel, J (2001). Replication-selective virotherapy for cancer: biological principles, risk management and future directions. *Nat Med* **7**: 781–787.
7. Kelly, E and Russell, SJ (2007). History of oncolytic viruses: genesis to genetic engineering. *Mol Ther* **15**: 651–659.
8. Kurooka, M and Kaneda, Y (2007). Inactivated Sendai virus particles eradicate tumors by inducing immune responses through blocking regulatory T cells. *Cancer Res* **67**: 227–236.
9. Fujihara, A, Kurooka, M, Miki, T and Kaneda, Y (2008). Intratumoral injection of inactivated Sendai virus particles elicits strong antitumor activity by enhancing local CXCL10 expression and systemic NK cell activation. *Cancer Immunol Immunother* **57**: 73–84.
10. Kawaguchi, Y, Miyamoto, Y, Inoue, T and Kaneda, Y (2009). Efficient eradication of hormone-resistant human prostate cancers by inactivated Sendai virus particle. *Int J Cancer* **124**: 2478–2487.
11. Tanaka, M, Shimbo, T, Kikuchi, Y, Matsuda, M and Kaneda, Y (2010). Sterile alpha motif containing domain 9 is involved in death signaling of malignant glioma treated with inactivated Sendai virus particle (HVJ-E) or type I interferon. *Int J Cancer* **126**: 1982–1991.
12. Matsushima-Miyagi, T, Hatano, K, Nomura, M, Li-Wen, L, Nishikawa, T, Saga, K *et al.* (2012). TRAIL and Noxa are selectively upregulated in prostate cancer cells downstream of the RIG-I/MAVS signaling pathway by nonreplicating Sendai virus particles. *Clin Cancer Res* **18**: 6271–6283.
13. Yoneyama, M, Kikuchi, M, Natsukawa, T, Shinobu, N, Imaizumi, T, Miyagishi, M *et al.* (2004). The RNA helicase RIG-I has an essential function in double-stranded RNA-induced innate antiviral responses. *Nat Immunol* **5**: 730–737.
14. Kato, H, Takeuchi, O, Sato, S, Yoneyama, M, Yamamoto, M, Matsui, K *et al.* (2006). Differential roles of MDA5 and RIG-I helicases in the recognition of RNA viruses. *Nature* **441**: 101–105.
15. Yount, JS, Kraus, TA, Horvath, CM, Moran, TM and López, CB (2006). A novel role for viral-defective interfering particles in enhancing dendritic cell maturation. *J Immunol* **177**: 4503–4513.
16. Kato, H, Takeuchi, O, Mikamo-Satoh, E, Hirai, R, Kawai, T, Matsushita, K *et al.* (2008). Length-dependent recognition of double-stranded ribonucleic acids by retinoic acid-inducible gene-I and melanoma differentiation-associated gene 5. *J Exp Med* **205**: 1601–1610.
17. Luo, D, Ding, SC, Vela, A, Kohlway, A, Lindenbach, BD and Pyle, AM (2011). Structural insights into RNA recognition by RIG-I. *Cell* **147**: 409–422.
18. Lu, C, Xu, H, Ranjith-Kumar, CT, Brooks, MT, Hou, TY, Hu, F *et al.* (2010). The structural basis of 5′ triphosphate double-stranded RNA recognition by RIG-I C-terminal domain. *Structure* **18**: 1032–1043.
19. Schmidt, A, Rothenfusser, S and Hopfner, KP (2012). Sensing of viral nucleic acids by RIG-I: from translocation to translation. *Eur J Cell Biol* **91**: 78–85.
20. Strahle, L, Garcin, D and Kolakofsky, D (2006). Sendai virus defective-interfering genomes and the activation of interferon-beta. *Virology* **351**: 101–111.
21. Baum, A and García-Sastre, A (2011). Differential recognition of viral RNA by RIG-I. *Virulence* **2**: 166–169.
22. Martínez-Gil, L, Goff, PH, Hai, R, García-Sastre, A, Shaw, ML and Palese, P (2013). A Sendai virus-derived RNA agonist of RIG-I as a virus vaccine adjuvant. *J Virol* **87**: 1290–1300.
23. Baum, A, Sachidanandam, R and García-Sastre, A (2010). Preference of RIG-I for short viral RNA molecules in infected cells revealed by next-generation sequencing. *Proc Natl Acad Sci USA* **107**: 16303–16308.
24. Johnston, MD (1981). The characteristics required for a Sendai virus preparation to induce high levels of interferon in human lymphoblastoid cells. *J Gen Virol* **56**: 175–184.
25. Takahasi, K, Yoneyama, M, Nishihori, T, Hirai, R, Kumeta, H, Narita, R *et al.* (2008). Nonself RNA-sensing mechanism of RIG-I helicase and activation of antiviral immune responses. *Mol Cell* **29**: 428–440.
26. Kaneda, Y (2010). Update on non-viral delivery methods for cancer therapy: possibilities of a drug delivery system with anticancer activities beyond delivery as a new therapeutic tool. *Expert Opin Drug Deliv* **7**: 1079–1093.
27. Kato, A, Ohnishi, Y, Kohase, M, Saito, S, Tashiro, M and Nagai, Y (2001). Y2, the smallest of the Sendai virus C proteins, is fully capable of both counteracting the antiviral action of interferons and inhibiting viral RNA synthesis. *J Virol* **75**: 3802–3810.
28. Kato, A, Cortese-Grogan, C, Moyer, SA, Sugahara, F, Sakaguchi, T, Kubota, T *et al.* (2004). Characterization of the amino acid residues of sendai virus C protein that are critically involved in its interferon antagonism and RNA synthesis down-regulation. *J Virol* **78**: 7443–7454.
29. Takeuchi, K, Komatsu, T, Kitagawa, Y, Sada, K and Gotoh, B (2008). Sendai virus C protein plays a role in restricting PKR activation by limiting the generation of intracellular double-stranded RNA. *J Virol* **82**: 10102–10110.
30. Holm, GH, Zurney, J, Tumilasci, V, Leveille, S, Danthi, P, Hiscott, J *et al.* (2007). Retinoic acid-inducible gene-I and interferon-beta promoter stimulator-1 augment proapoptotic responses following mammalian reovirus infection via interferon regulatory factor-3. *J Biol Chem* **282**: 21953–21961.
31. Goubau, D, Schlee, M, Deddouche, S, Pruijssers, AJ, Zillinger, T, Goldeck, M *et al.* (2014). Antiviral immunity via RIG-I-mediated recognition of RNA bearing 5′-diphosphates. *Nature* **514**: 372–375.
32. Marques, JT, Devosse, T, Wang, D, Zamanian-Daryoush, M, Serbinowski, P, Hartmann, R *et al.* (2006). A structural basis for discriminating between self and nonself double-stranded RNAs in mammalian cells. *Nat Biotechnol* **24**: 559–565.
33. Dufour, JH, Dziejman, M, Liu, MT, Leung, JH, Lane, TE and Luster, AD (2002). IFN-gamma-inducible protein 10 (IP-10; CXCL10)-deficient mice reveal a role for IP-10 in effector T cell generation and trafficking. *J Immunol* **168**: 3195–3204.
34. Angiolillo, AL, Sgadari, C, Taub, DD, Liao, F, Farber, JM, Maheshwari, S *et al.* (1995). Human interferon-inducible protein 10 is a potent inhibitor of angiogenesis in vivo. *J Exp Med* **182**: 155–162.
35. Kaneda, Y, Nakajima, T, Nishikawa, T, Yamamoto, S, Ikegami, H, Suzuki, N *et al.* (2002). Hemagglutinating virus of Japan (HVJ) envelope vector as a versatile gene delivery system. *Mol Ther* **6**: 219–226.